PHYSICAL REVIEW B **84**, 115401 (2011)

Making angle-resolved photoemission measurements on corrugated monolayer crystals: Suspended exfoliated single-crystal graphene

Kevin R. Knox,[1,2] Andrea Locatelli,[3] Mehmet B. Yilmaz,[4] Dean Cvetko,[5,6] Tevfik Onur Menteş,[3] Miguel Ángel Niño,[3,7] Philip Kim,[1] Alberto Morgante,[5,8] and Richard M. Osgood Jr.[2]

[1]*Department of Physics, Columbia University, New York, New York, USA*
[2]*Department of Applied Physics, Columbia University, New York, New York, USA*
[3]*Elettra–Sincrotrone Trieste S.C.p.A., Basovizza, Trieste, Italy*
[4]*Department of Physics, Fatih University, Istanbul, Turkey*
[5]*CNR-IOM, Laboratorio Nazionale TASC, Trieste, Italy*
[6]*Faculty for Mathematics and Physics, University of Ljubljana, Ljubljana, Slovenia*
[7]*Instituto Madrileño de Estudios Avanzados IMDEA Nanociencia, Cantoblanco, E-28049 Madrid, Spain*
[8]*Department of Physics, Trieste University, I-34127 Trieste, Italy*

(Received 5 April 2011; revised manuscript received 23 June 2011; published 1 September 2011)

Free-standing exfoliated monolayer graphene is an ultrathin flexible membrane, which exhibits out-of-plane deformation or corrugation. In this paper, a technique is described to measure the band structure of such free-standing graphene by angle-resolved photoemission. Our results show that photoelectron coherence is limited by the crystal corrugation. However, by combining surface morphology measurements of the graphene roughness with angle-resolved photoemission, energy-dependent quasiparticle lifetime and band-structure measurements can be extracted. Our measurements rely on our development of an analytical formulation for relating the crystal corrugation to the photoemission linewidth. Our angle-resolved photoemission spectroscopy measurements show that, despite significant deviation from planarity of the crystal, the electronic structure of exfoliated suspended graphene is nearly that of ideal, undoped graphene; we measure the Dirac point to be within 25 meV of E_F. Further, we show that suspended graphene behaves as a marginal Fermi liquid, with a quasiparticle lifetime that scales as $(E - E_F)^{-1}$; comparison with other graphene and graphite data is discussed.

DOI: 10.1103/PhysRevB.84.115401 PACS number(s): 73.22.Pr, 68.65.Pq

I. INTRODUCTION

The recent availability of monolayer-thick two-dimensional crystals such as graphene, boron nitride (BN), and bismuth strontium calcium copper oxide (BSCCO) has generated widespread interest in the physics and materials science communities. In the case of graphene, in particular, the two-dimensional nature of the crystal in combination with its unusual massless Dirac fermions determines a host of intriguing and unique transport phenomena, including graphene's half integer quantum Hall effect (HE) and nonzero Berry's phase.[1,2] Unlike most metals, undoped graphene has a Fermi surface that consists of a set of two inequivalent points in momentum space. Thus at zero temperature and zero doping, the density of states at the Fermi level vanishes. In combination with the linear dispersion of low-energy charge carriers, this vanishing density of states is expected to lead to unusual band-renormalization effects that are not seen in Fermi-liquid systems such as unusually high electron-electron coupling. Motivated by interest in these unusual properties, several theoretical and experimental studies have investigated the electronic properties of graphene.[3]

Angle-resolved photoemission spectroscopy (ARPES) is the experimental method that is most frequently used to probe the electronic structure of crystals. However, so far, the majority of ARPES studies of graphene have been conducted on epitaxial graphene, which has been grown on a variety of substrates such as SiC, Ru, Ni, and Ir.[4–11] Epitaxial graphene is ideal for photoemission experiments, but, due to the interaction between the epitaxial graphene monolayer and the substrate, the band structure is often distorted such that the Dirac point shifts away from the Fermi energy, thus changing the quasiparticle dynamics. In an effort to minimize the effect of substrate interaction on epitaxial graphene, recent ARPES studies have focused on several multilayer systems, such as intercalated graphite[12] and graphene grown on the C face of SiC.[13] These layered systems consist of multiple stacked graphene sheets that are substantially electrically isolated, thus resulting in an electronic band structure that mimics that of suspended exfoliated single-layer graphene. However, despite its scientific and technological importance, exfoliated graphene has been the subject of only a limited number of ARPES studies,[9,14] despite the fact that it remains the best choice for device physics, as it is easily backgated and has the highest measured mobility.[15]

Several obstacles impede measurement of the band structure of exfoliated graphene. One difficultly arises from the fact that available single-layer exfoliated graphene flakes are typically less than 20 μm in size, thus precluding the use of standard ARPES systems, which require samples to be several mm in size. Hence most information regarding low-energy occupied states in exfoliated graphene has been obtained indirectly from electrical-transport measurements[1,2] or directly by optical-probing techniques.[16,17] These techniques examine the band structure generally within 1 eV of the Dirac point and do not directly provide momentum resolution. For photoemission the limitation in size can be overcome by working with high lateral-spatial-resolution probes such as those available using spectromicroscopy.[11,18] A second major impediment to photoemission studies is due to the fact

 ©2011 American Physical Society

that graphene is an ultrathin crystal. This ultrathin property has, in turn, two important consequences for photoemission studies. The first is the transparency of monolayer graphene to UV photons and photoemitted electrons, which causes a strong background photoemission signal if the monolayer graphene is in close physical proximity with a substrate.[14] The second is that exfoliated graphene is not atomically flat, but is known to deform locally, a result shown through atomic force microscopy (AFM), scanning tunneling microscopy (STM), electron microscopy, and electron-scattering results.[19–23] It has been argued that the deformation is due to the fact that monolayer-thick graphene has soft flexural modes leading to ready bending of the graphene. The presence of a supporting substrate or scaffold can, to a certain degree, stabilize height fluctuations in the graphene layer, but corrugations in the underlying supporting substrate are transferred in part to the graphene due to the reduced stiffness of this material. Additionally, intrinsic corrugations that cannot be attributed to interaction with the substrate were recently observed in supported graphene.[19] Further, in a recent low-energy diffraction study, we demonstrated that even graphene suspended over etched cavities exhibits corrugation, which appeared to have been intrinsic in origin.[21]

Thus, in general, two-dimensional (2D) crystals produced by exfoliation may show significant local curvature, manifested as corrugation and ripples. This corrugation is known to affect not only the electronic and transport properties of the material, but can also have a major impact on photoemission results. In particular, the theory of ARPES was developed for single-crystal atomically flat surfaces and relies on the fact that momentum perpendicular to the surface is conserved in the photoemission process. On such perfectly ordered crystals the photoemission line shape is directly related to the spectral function of the electronic state being probed, from which information about many-body physics can be extracted. The corrugation in thin sheets of layered materials breaks this symmetry and obscures the intrinsic many-body effects.

In this paper, we present a systematic approach to account for such corrugation-induced broadening in ARPES on thin films. By combining our photoemission results with detailed information about surface morphology obtained from prior electron-microscopy measurements[21] taken *in situ* on the same samples we are able to quantify the influence of corrugation on spectral broadening. We go on to describe a method to discount the effect of surface corrugation from ARPES measurements to reveal the intrinsic many-body physics present in graphene. Our results show that suspended graphene behaves as a marginal Fermi liquid with an anomalous quasiparticle lifetime, which scales as $(E - E_F)^{-1}$.

II. EXPERIMENT

Our measurements used the Spectroscopic Photoemission and Low Energy Electron Microscope (SPELEEM) at the Nanospectroscopy beamline at the Elettra Synchrotron light source.[24] The SPELEEM is a versatile multitechnique microscope that combines low-energy electron microscopy (LEEM) with energy-filtered x-ray photoemission electron microscopy (XPEEM). The microscope images surfaces, interfaces, and ultrathin films using a range of complementary analytical characterization methods, which have been described in detail previously.[25,26] When operated as a LEEM, the microscope probes the specimen using elastically backscattered electrons. LEEM enables high sensitivity to surface crystalline structure and, due to the favorable backscattering cross sections of most materials at low energies, allows image acquisition to be obtained at video frame rate. The lateral resolution of the microscope for LEEM imaging is currently below 10 nm. In XPEEM mode, the specimen is probed using the beamline photons, provided by an undulator source; thus the technique is sensitive to the local chemical and electronic structures. Laterally resolved versions of synchrotron based absorption (XAS) and photoemission spectroscopy (XPS) are possible. The lateral resolution in XPEEM approaches a few tens of nm.[27]

Along with real-space imaging, the SPELEEM microscope is capable of microprobe diffraction imaging, i.e., laterally restricted low-energy electron diffraction (μ-LEED) and angle-resolved photoemission electron spectroscopy (μ-ARPES) measurements when probing with electrons and photons, respectively. In diffraction operation the microscope images and magnifies the back focal plane of the objective lens. In ARPES mode, the full angular emission pattern can be imaged on the detector up to a parallel momentum of ~ 2 Å^{-1}; at larger parallel momentum the transmission of the microscope decreases. All diffraction measurements are restricted to areas of ~ 2 μm in diameter, which are selected by inserting a field limiting aperture into the first image plane along the imaging-optics column of the instrument. Thus the microscope enables measurements on samples that are homogeneous over areas of a few square μm.

The energy resolution of the SPELEEM is 300 meV and the momentum resolution of the microscope when operated in diffraction mode (LEED or ARPES) is ~ 0.045 Å^{-1}. This value for the momentum resolution was obtained from calibration on a standard tungsten crystal; measurements using this crystal showed that the value changed by less than 5% as the kinetic energy of photoemitted electrons (or backscattered electrons for the case of LEED) increased from 25 to 100 eV. Specifically, the momentum resolution was observed to increase from 0.044 Å^{-1}at 25 eV to 0.046 Å^{-1}at 100 eV.

Graphene samples were extracted by micromechanical cleavage from Kish graphite crystals (Toshiba Ceramics, Inc.) and placed onto an SiO_2-thin-film layer on an Si substrate, which was previously patterned with cylindrical cavities to a depth of 300 nm, as described in Ref. 21. The use of planar processing of this substrate allowed us to suspend areas of the graphene films without the use of further photolithographic techniques, which would introduce contaminants to the graphene sheets. Graphene samples with lateral sizes from 10 to 50 μm were placed in contact with Au grounding strips deposited on the surface via thermal evaporation through a shadow mask. A sketch of the sample configuration is shown in Fig. 1 along with an optical micrograph.

The microscope used to collect data has the important advantage of having a sufficiently high spatial resolution to guarantee that we are measuring a single-crystal sample of monolayer graphene and that all of the measured spectral intensity is derived from a fully suspended region. This capability is necessary since the suspended regions are

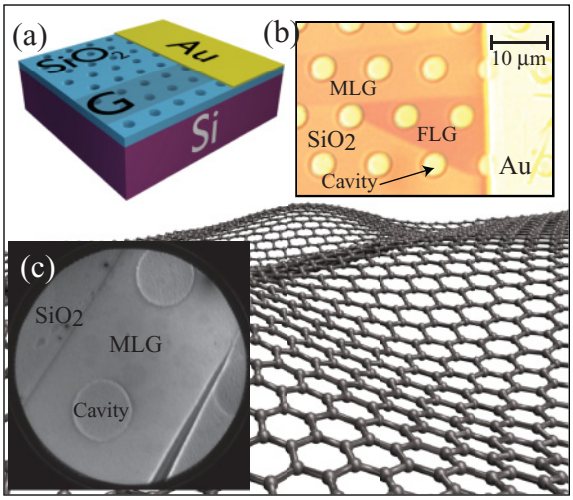

FIG. 1. (Color online) (a) Schematic drawing of our suspended-graphene sample configuration. (b) Optical micrograph of sample containing suspended monolayer graphene (MLG) and few-layer graphene (FLG). (c) LEEM image at 1.3 eV of typical sample area of interest. (Background) Artist's rendering of corrugated graphene crystal (height fluctuations not to scale).

approximately 5 μm in diameter and therefore cannot be resolved with conventional photoemission instruments, which employ spatial averaging techniques that collect data over surface areas of several square millimeters. The potential to combine both photoemission and electron-scattering measurements is essential for our experiment since it allows us to measure band structure and surface morphology on the same samples. We note, additionally, that a similar instrument was recently used in a study, which examined the morphology and electronic structure of epitaxial graphene grown on Pt.[11]

After preparation the samples were placed into a UHV chamber with a base pressure of 2×10^{-10} mbar, and the surface cleaned via low-energy electron irradiation to eliminate adventitious hydrocarbon molecules adsorbed during prior atmospheric exposure.[21] All graphene samples were characterized with LEEM before investigation with ARPES and LEED. For each sample, LEEM was used to locate sample areas of interest and to determine film thickness with atomic resolution by measuring intensity modulations in the LEEM *I-V* spectra.[21,28,29]

ARPES data at multiple photon energies were obtained on the suspended areas of the graphene film. Only regions of uniform thickness were considered. In order to elucidate the role of surface corrugation and substrate influence, comparative experiments were also carried out on corresponding regions where the film was supported by the SiO_2 substrate. This surface has been recently carefully calibrated by prior STM and electron-scattering measurements.[19,20,22] In addition, ARPES measurements were made on Kish-graphite flakes that were present on the same substrates. As graphite is a well understood and commonly studied system, these measurements provided a useful point of comparison for our graphene measurements. Photoemission from graphite is, in some respects, similar to that from graphene because of the stacked-layer nature of the former. However, the physics near the Dirac point is significantly different owing to the fact that the multilayer stacking in graphite breaks the symmetry between *A* and *B* sublattices, which results in two dispersing branches, such that low-energy excitations do not have the simple linear dispersion relation that is found for graphene.

III. RESULTS

Photoemission spectra were measured from two samples with differing degrees of surface corrugation and substrate interaction, that is, on suspended and substrate-supported graphene; note that all ARPES data presented in the paper are raw (*i.e.* unprocessed) unless explicitly stated otherwise. Previous LEED measurements have shown that the horizontal correlation length increases from 24 to 30 nm in measurements taken on supported and suspended samples, respectively.[21] In addition, ARPES data were collected at room temperature over the entire surface Brillouin zone (SBZ) from 0.5 eV to −8 eV (energy referenced to E_F), for monolayer graphene and graphite, using a range of photon energies. Figure 2 shows ARPES spectra taken from a sample supported by and in contact with the SiO_2 surface and a sample that was suspended over the 5-μm wells shown in Fig. 1. For comparison, the ARPES spectrum from Kish graphite is shown as well. These data have been included to provide an example of the photoemission linewidth obtained by the SPELEEM instrument on a well-known and related crystal system.

The data show dispersion along three symmetry lines in the SBZ. As expected from the reduced corrugation, as well as the absence of any substrate interaction, the ARPES data for suspended graphene show a dramatic improvement in quality as compared to the data for supported graphene. Additionally, there is a very broad, parabolically dispersing peak centered at the Γ point at a binding energy of ∼8 eV in

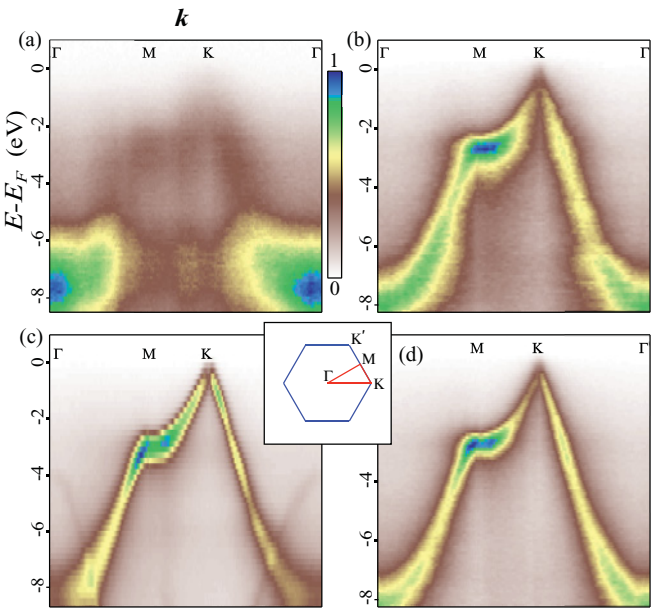

FIG. 2. (Color online) ARPES data along symmetry directions in Brillouin zone for graphene and graphite. (a) SiO_2 supported graphene ($\hbar\omega = 90$ eV). (b) Suspended graphene ($\hbar\omega = 84$ eV). (c) Kish graphite ($\hbar\omega = 90$ eV). (d) Suspended graphene ($\hbar\omega = 50$ eV). Inset shows 2D graphene Brillouin zone.

the data taken on *supported* graphene. This feature has been previously attributed to photoemission from the amorphous SiO_2 substrate[14] and is not observed in the spectrum taken on suspended graphene. Although the substrate is only 300 nm below the suspended graphene, any background electrons emitted at this height will be significantly defocused in the electron optics of the SPELEEM microscope. Additionally, due to the grazing incidence angle of the photon beam (16°), the bottom of the cavity is not fully illuminated as the cavity edge casts a shadow, which further reduces the photoemission signal from the substrate.

In the vicinity of the K points, a conical dispersion is observed centered at the K point on the suspended graphene spectrum. At ∼1 eV below the Fermi level a trigonal-warping deviation from angular isotropy becomes clearly noticeable. Measurements taken through the K point and in the vertical direction (perpendicular to the ΓK direction) show two symmetric dispersing branches forming the two sides of the Dirac cone. The band structure can be made significantly sharper (see Fig. 3) by taking the second derivative along each momentum direction. In this case, use of the second derivative allows easier determination of the Dirac point with respect to the Fermi level. Figure 3(b) shows the linear best fit to the two branches as well as the location of the Fermi level. From the fit, we find that the Dirac point is within 25 meV of E_F ($E_D = -9 \pm 25$ meV). Thus the sample is minimally doped

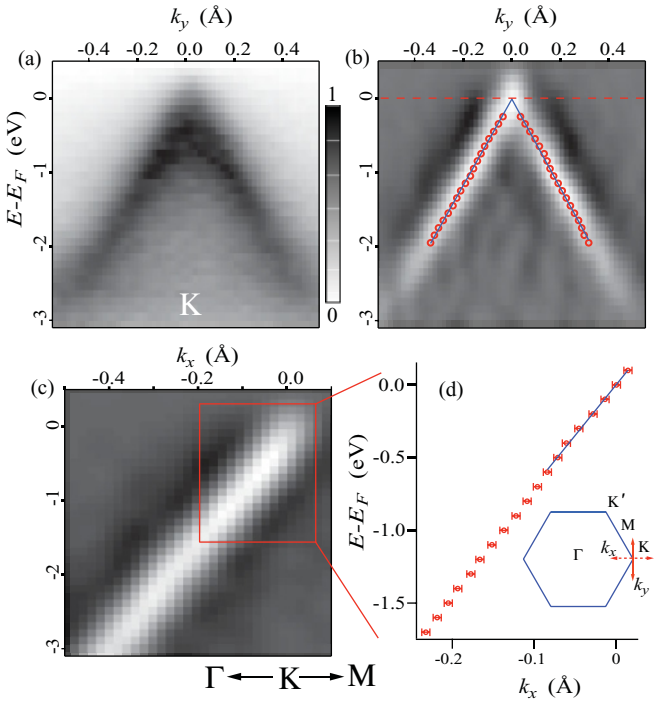

FIG. 3. (Color online) (a) ARPES intensity through K point along k_y direction (perpendicular to ΓK direction) in suspended monolayer graphene ($\hbar\omega = 50$ eV). (b) Smoothed second derivative image of dispersion shown in (a). Dashed red line indicates Fermi level. Red circles indicate peak positions and solid blue lines represent best fit to the dispersion. (c) Smoothed second derivative ARPES intensity through K point along k_x (ΓK) direction. (d) Extracted dispersion from (c). Inset shows graphene Brillouin zone. Red solid (dashed) line indicates k_y (k_x) direction through K point.

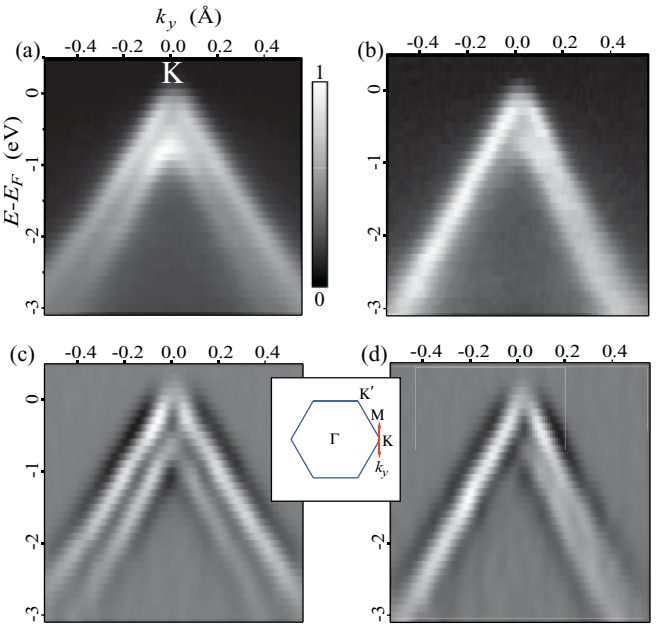

FIG. 4. (Color online) Dispersion along the k_y direction (defined as shown in the inset) through the $\bar{K}$ point for graphite obtained at photon energies of (a) $\hbar\omega = 86$ eV and (b) $\hbar\omega = 76$ eV. (c),(d) Smoothed second derivative images of spectra shown in (a) and (b), respectively. Inset shows graphite surface Brillouin zone. Solid red line indicates k_y direction through $\bar{K}$ point.

due to the preparation procedure used here, which did not involve any photolithographic or chemical-transfer techniques. In contrast, the Dirac point previously measured by our group on a supported sample was found to be ∼300 meV below the Fermi level, which was attributed to doping by interaction with charged impurities in the SiO_2 layer.[14]

For comparison with results on a known 3D photoemission materials system, graphite spectra were taken at two photon energies (86 and 76 eV) along the same (vertical) direction through the K point; these results are shown in Fig. 4. Additionally, these data allow us to display the instrumental resolution on this known system. The dispersion obtained at $\hbar\omega = 86$ eV is clearly symmetric about the K point. At this photon energy we can resolve the splitting of the π state into bonding and antibonding bands, with the two bands separated by ∼0.12 Å^{-1}. The bands themselves are approximately 0.1 Å^{-1} in width. In the spectrum taken at 76 eV the two peaks are nearly degenerate. Again, the second derivative allows for easier determination of peak locations.

Figure 5 shows the graphene dispersion taken along the ΓK direction through the K point. Comparative measurements were made at two different photon energies ($\hbar\omega = 50$, $\hbar\omega = 84$) and are shown in Figs. 5(a) and 5(b), respectively. In this direction, only one branch of the dispersion can be seen as the difference in phase between electron waves emitted from the A and B sublattice sites results in complete destructive interference.[30] Thus this is a convenient direction along which to measure precisely the dispersion in the vicinity of the Dirac cone. The inset to Fig. 5(c) compares momentum distribution curves (MDCs) taken at a binding energy of 0.7 eV for the suspended-graphene spectra at both photon energies. The data in Fig. 5(c) show that the width of the $\hbar\omega = 84$-eV MDC is

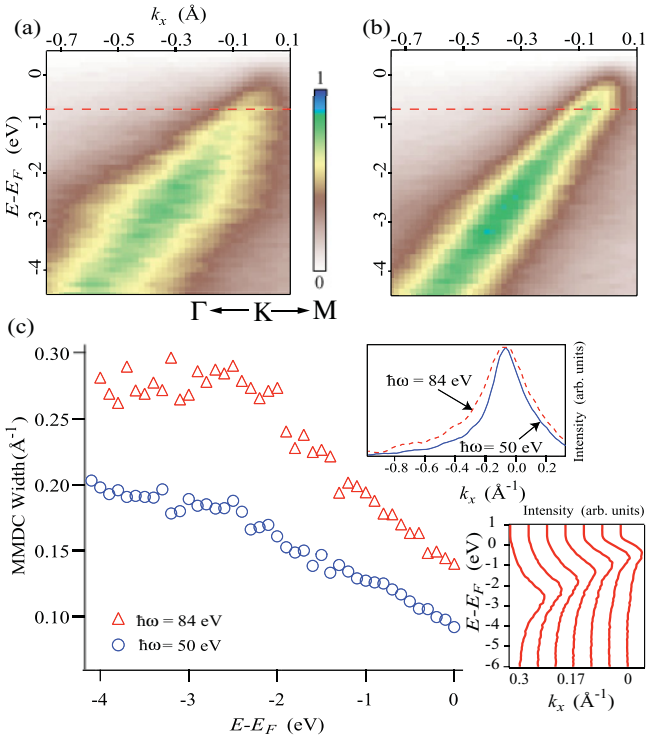

FIG. 5. (Color online) ARPES intensity along ΓK direction in suspended monolayer graphene. Graphene photoemission taken with photon energies of (a) $\hbar\omega = 50$ eV and (b) $\hbar\omega = 84$ eV. (c) Half width at half maximum of MDCs as a function of binding energy taken from (a) and (b). Upper inset shows sample MDCs taken 0.7 eV below E_F as indicated by dashed red lines in (a) and (b). Lower inset shows sample EDCs taken from $\hbar\omega = 50$-eV data set. Successive EDCs separated by ∼0.057 Å^{-1}.

significantly larger than the $\hbar\omega = 50$ eV MDC (0.17 Å^{-1} vs 0.12 Å^{-1}).

Additionally, there is a slight asymmetry in all three MDCs as additional spectral weight is present on the right side of the peak (at higher values of k_x). The background signal decreases and the peaks become narrower for 50-eV photons as compared to 84-eV photons. Specifically, in the 0–4-eV range (referenced to E_F), the MDC width increases monotonically from 0.1 to 0.2 Å^{-1} and from 0.15 to 0.3 Å^{-1} for data collected with 50- and 84-eV photons, respectively. In contrast, MDCs taken along the same direction (ΓK) on supported graphene are significantly broader[14] and show almost no dependence on binding energy; they are ∼0.5 Å^{-1} in width from the Fermi energy to −4 eV binding energy. Thus spectral features are sharpest for suspended samples measured with lower photon energy.

Referring, now, to data taken on the suspended sample, one obvious concern is that the dramatic increase in spectral features observed with increasing photon energy reflects an electron kinetic-energy dependence in the momentum resolution of the instrument. However, as noted above the instrumental resolution has been calibrated with a standard tungsten crystal and shown to increase by less than 5% over a large range in electron kinetic energies (25–100 eV). This change in resolution is not sufficient to explain the ∼50% increase seen in MDC width between data taken with 50- and 84-eV photons. Additionally, as noted above, one can clearly resolve features that are separated by less than 0.12 Å^{-1} in the graphite spectrum obtained with a photon energy of 86 eV.

IV. DISCUSSION

A. Comparison of graphite and graphene results

As shown in Fig. 5, variation in photon energy results in changes to the linewidth of the graphene photoemission spectra, which can be exploited to sharpen the spectrum. In explaining these results on graphene, it is useful first to examine the effect of photon energy variation for the case of *graphite*. The differences in the measured photemission spectra of graphite taken at $\hbar\omega = 76$ eV and $\hbar\omega = 86$ eV shown in Figs. 4(a) and 4(b), respectively, are easily understood to be the result of the three-dimensional band structure of graphite; namely, a change in photon energy causes a change in k_z, which is manifest in the spectra in Fig. 4 as a decrease in the band splitting.[30–35]

Consider now the effect of changing photon energies for the case of graphene photoemission. Since graphene is truly a 2D crystal, the initial states in the valence band are highly localized along the z direction. Thus the Brillouin zone is strictly two dimensional and the electronic structure is essentially k_z independent. Comparison with photoemission from surface states is useful, since they are also localized in two dimensions.[36] However, the role of evanescent decay into the bulk, which is important for surface states in metals and results in a partial k_z dependence,[36] such as surface resonance, is absent in graphene and thus we may treat the initial state as independent of photon energy. In fact, as seen in Fig. 5, changing the photon energy in the case of graphene causes only a change in the overall linewidth and does not affect the measured band structure. As will be discussed below, the difference in the width of ARPES features between spectra obtained at $\hbar\omega = 50$ and $\hbar\omega = 84$ is a consequence of the surface roughness of the graphene samples. Since electrons in graphene propagate on a locally curved surface, the usual momentum conservation rules in ARPES must be modified and a photon-energy-dependent broadening term is introduced.

B. General considerations

In standard many-body ARPES theory, the intensity of the photoemission signal is proportional to the spectral function $A(\mathbf{k},\omega)$:

$$A(\mathbf{k},\omega) = \frac{\mathrm{Im}[\Sigma(\mathbf{k},\omega)]}{\{\omega - \omega_{\mathbf{k}} - \mathrm{Re}[\Sigma(\mathbf{k},\omega)]\}^2 + \mathrm{Im}[\Sigma(\mathbf{k},\omega)]^2}, \quad (1)$$

where $\omega = E - E_F$ and $\mathbf{k}$ are binding energy and momentum, respectively, and $\omega_{\mathbf{k}}$ is the single-particle dispersion. The real and imaginary parts of the self-energy $\Sigma(\mathbf{k},\omega)$ represent renormalization of the bare bands and scattering rate, respectively. To obtain the full expression for the photocurrent, the above function is then multiplied by energy and momentum-preserving δ functions, $\delta(\mathbf{k}_i - \mathbf{k}_f - \mathbf{G})\delta(E_i - E_f - W)$, where $\mathbf{G}$ is a reciprocal-lattice vector and i and f label the initial and final states, respectively, and W is the work function of the material.

However, one major complication to this approach arises for the case of suspended graphene since the momentum

preserving function $\delta(\mathbf{k}_i - \mathbf{k}_f - \mathbf{G})$ is only a precise δ function if the system under investigation is atomically flat. While this is the case for the majority of single-crystal samples probed with ARPES, including the Kish graphite described above, exfoliated monolayer graphene, as is discussed in the Introduction, has significant deviations from planarity, ranging from 1 to 10 Å.[37] This corrugation introduces an additional broadening mechanism into the ARPES spectrum, which can be as large as, or larger than, the intrinsic broadening represented by $\mathrm{Im}[\Sigma(\mathbf{k},\omega)]$. Thus in order to extract the true self-energy of carriers in the crystal, such corrugation-induced broadening must be taken into account. The MDCs are best fit by a convolution of $A(\mathbf{k},\omega)$ with a function that represents broadening due to surface roughness. Thus, as will be shown below, at fixed ω, photoemission intensity as a function of $\mathbf{k}_\parallel$ can be expressed as

$$I(\mathbf{k}_\parallel) \propto \int d^2k_\parallel{}' S_{k_\perp}(\mathbf{k}_\parallel) A(\mathbf{k}_\parallel - \mathbf{k}'_\parallel, \omega), \qquad (2)$$

where $\mathbf{k}_\parallel = \mathbf{k}_{i\parallel} - \mathbf{k}_{f\parallel}$ and $S_{\mathbf{k}_\perp}$ represents corrugation-induced broadening. $S_{\mathbf{k}_\perp}$, the surface structure factor, is a function of the surface geometry of the sample and is also generally dependent on the change in perpendicular momentum from initial to final state, $k_\perp = k_{i\perp} - k_{f\perp}$. We note that several prior studies have examined the effect of surface roughness on ARPES measurements.[38,39] In these prior studies, the roughness considered was due to discrete height variations caused by monatomic steps, rather than the continuous undulations of a thin film. Thus the broadening in spectral features measured by ARPES was attributed to increased electron scattering rather than a variation in the phase of photoemitted electrons induced by local height fluctuations. In our experiments on suspended graphene samples, the surface morphology is carefully measured simultaneously with the ARPES measurements presented here, thus allowing us to determine $S_{\mathbf{k}_\perp}$ independently.[27]

Finally, note that the surface corrugation of the graphene sheets will also alter the band structure by inducing a change in the local potential proportional to the square of the curvature. Thus the ripples act as scattering centers, which will decrease lifetime and potentially change the Fermi velocity. These effects are contained in $A(\mathbf{k},\omega)$ and will also be present in the ARPES data. However, such effects are distinct from that described by $S_{k_\perp}$, which represents decoherence as electrons pass from a curved 2D space to free space.

C. Corrugation broadening

Corrugation broadening can be treated by considering the equation that describes photoemission from a Bloch state in the graphene sheet into a free-electron state above the crystal. Using the standard tight-binding approach to describe the initial state,

$$\psi_{\mathbf{k}}(\mathbf{r}) = \frac{1}{\sqrt{N}} \sum_{\mathbf{R}} e^{i\mathbf{k}\cdot\mathbf{R}} \sum_{j=A,B} C_j^{\mathbf{k}} \phi(\mathbf{r} - \mathbf{R} - \tau_j), \qquad (3)$$

we obtain the following matrix element for excitation into a free-electron final state:

$$M \propto (\mathbf{k_i} \cdot \hat{\lambda}) \sum_{j=A,B} C_j^{\mathbf{k_i}} e^{-i\mathbf{k_f}\cdot\tau_j} \sum_R e^{i(\mathbf{k_i}-\mathbf{k_f})\cdot\mathbf{R}} \tilde{\phi}(\mathbf{k_f}), \qquad (4)$$

where $\mathbf{k_i}$ is the initial pseudomomentum of a valence-band electron and $\mathbf{k_f}$ is the final-state momentum (for a full description and definitions of symbols see the Appendix). Equation (3) describes an initial state with precise momentum at a fixed binding energy. For an atomically flat crystalline 2D surface the position vectors can be expressed as $\mathbf{R} = n_1\mathbf{a}_1 + n_2\mathbf{a}_2$, where the n_i are integers and the $\mathbf{a}_i$ are primitive lattice vectors in the xy plane. In this case, the sum over $\mathbf{R}$ in Eq. (3), $\sum e^{i(\mathbf{k_i}-\mathbf{k_f})\cdot\mathbf{R}}$, is zero unless $\mathbf{k_{i\parallel}} - \mathbf{k_{f\parallel}} = \mathbf{G}$, where $\mathbf{G}$ is a reciprocal-lattice vector. This condition is thus a statement of the momentum conservation discussed above, $\delta(\mathbf{k_i} - \mathbf{k_f} - \mathbf{G})$. If, however, z is allowed to vary continuously as a function of position along the surface, so that $\mathbf{R} = n_1\mathbf{a}_1 + n_2\mathbf{a}_2 + \Delta x + \Delta y + z$,[40] with z no longer constant, the summation in Eq. (4) is not as readily calculated. Perfect phase cancellation away from reciprocal-lattice vectors does not occur, resulting in nonzero photoemisison intensity when $\mathbf{k_{i\parallel}} - \mathbf{k_{f\parallel}} \neq \mathbf{G}$.

Summations such as the one in Eq. (4) are encountered in the theory of LEED on rough surfaces.[41–43] In fact, in many respects the formal analysis of LEED results bears many similarities to that of ARPES. In a prior study using one-photon photoemission and high-resolution LEED applied simultaneously to surface states of Cu(100) and Cu(111), it was demonstrated experimentally that the photoemission linewidth and the width of the LEED-spot profile are correlated linearly.[39] In particular, for LEED one measures the diffraction structure factor, $S(\mathbf{k}) \propto |\sum \mathbf{e^{ik\cdot R}}|^2$ where, as in the case of photoemission, $\mathbf{k}$ is the total momentum transfer, $\mathbf{k} = \mathbf{k_i} - \mathbf{k_f}$, and the sum is over atomic positions $\mathbf{R}$ on a surface. In addition, for ARPES transition probability is proportional to the square of the matrix element; thus the same structure factor $S(\mathbf{k})$ is applicable. Thus LEED theory can guide our analysis.

The structure factor $S(\mathbf{k})$ can be calculated with information about the average properties of the surface, described by three variables: horizontal correlation length ξ, rms height variation w, and a dimensionless parameter α, termed the "roughness exponent," which describes surface roughness on length scales smaller than ξ.[43] All three parameters can be extracted from real-space information about the surface by computing the height-height correlation function, which is used in a variety of thin-film measurements, including those on graphene and other surfaces, and is defined as $H(r) = \langle |z(r_0 + r) - z(r_0)|^2 \rangle$. As is shown in the Appendix, $S(\mathbf{k}) = S(k_\perp, \mathbf{k}_\parallel)$ is intimately related to $H(r)$ as the Fourier transform of $e^{-(1/2)k_\perp H(r)}$. Thus the average parameters that characterize a given rough surface (w, ξ, and α) and determine the form of $H(r)$ also determine $S(k_\perp, \mathbf{k}_\parallel)$. Hence with these parameters, it is possible to compute the summation in Eq. (4). In fact, previously reported measurements using LEEM and LEED have determined these parameters to be $\alpha = 0.54 \pm 0.02$, $w = 1.99 \pm 0.15$ Å, and $\xi = 30 \pm 0.3$ nm for the same suspended graphene samples used in this study.[21] Although the functional form of $S(k_\perp, \mathbf{k}_\parallel)$ is complex, the width of $S_{k_\perp}(\mathbf{k}_\parallel)$ (i.e., for $k_\perp$ fixed) in $\mathbf{k}_\parallel$ space has a simple dependence on $k_\perp$ and the parameters describing the surface roughness. In particular, the width Γ_S is proportional to $(k_\perp w)^{1/\alpha}/\xi$, which explains the decrease in experimental linewidth with decreasing $k_\perp$ shown in Fig. 5. For fitting purposes it is useful to have the exact functional form of $S_{k_\perp}(\mathbf{k}_\parallel)$. Yang *et al.* have shown that for

$(wk_\perp)^2 \gg 1$ the form is purely diffusive and can be expressed as[43]

$$S_{k_\perp}(\mathbf{k}_\parallel) = [\xi/(wk_\perp)^{1/\alpha}]F_\alpha[\mathbf{k}_\parallel\xi/(wk_\perp)^{1/\alpha}]$$
$$F_\alpha(Y) = \int XdX\exp(-X^{2\alpha})J_0(XY). \quad (5)$$

D. Intrinsic broadening

It is straightforward to introduce intrinsic initial-state broadening into our ARPES description by replacing our initial state wave function $\psi_\mathbf{k}$ with a sum over multiple momentum states, $\sum a_\mathbf{k}\psi_\mathbf{k}$, where the $a_{\mathbf{k}_i}$ are complex coefficients related to the spectral function by $|a_{\mathbf{k}_i}|^2 = A(\mathbf{k},\omega)$. Our transition matrix then becomes a sum, $M = \sum a_\mathbf{k} M^\mathbf{k}$, over multiple matrix elements weighted by the complex coefficients $a_\mathbf{k}$, where the $M^\mathbf{k}$ are the original transition matrix elements defined in Eq. (4). Again, using Fermi's golden rule we find that the transition probability is proportional to the square of this sum,

$$I \propto |M|^2 = \left|\sum_k a_k M^\mathbf{k}\right|^2$$
$$= \sum_\mathbf{k} |a_\mathbf{k}|^2|M^k|^2 + \sum_{\mathbf{k}\neq\mathbf{k}'} a^*_\mathbf{k} a_{\mathbf{k}'} M^{\mathbf{k}*} M^{\mathbf{k}'}. \quad (6)$$

As shown in the Appendix the $\mathbf{k} \neq \mathbf{k}'$ sum can be safely neglected due to random phase cancellation and we arrive at the final expression for the full photoemission intensity expressed in Eq. (2).

Note that the broadening introduced by the surface corrugation of the suspended graphene sheet is *only* contained in the transition matrix element M^k. The many-body physics that describes the interaction of charge carriers in graphene with other excitations is contained in the complex coefficients $a_\mathbf{k}$. Thus the "intrinsic" or initial-state broadening referred to in this section, as well as in subsequent sections, is the width of the spectral function derived from the complex coeffiecients, $A(\mathbf{k},\omega) = |a_{\mathbf{k}_i}|^2$.

E. Analysis of spectra and discussion

Figure 3(d) shows a plot of the dispersion obtained along the ΓK direction in the vicinity of the Dirac point. The average Fermi velocity, derived from the slope of ω vs k_x, is $1.07 \pm 0.05 \times 10^6$ m/s. This value is obtained from an analysis of the dispersion in the energy range from 0 to 0.6 eV [see blue best-fit line in Fig. 3(d)]. Additionally, the dispersion along ΓK is linear in this region (0–0.6 eV) with no deviations from linearity within our experimental uncertainty. As discussed above, despite the roughness induced broadening in the spectrum, the dispersion curve is easily extracted from the ARPES data by taking the second derivative of the ARPES intensity along the momentum direction. However, determining the intrinsic width of spectral features requires a deeper analysis.

Our prior measurements of the surface corrugation in suspended graphene allow us to extract the intrinsic electronic structure from our ARPES data. The procedure for this fitting is as follows: first, $S_{k_\perp}$ is determined from our surface morphology measurements and used as a constant parameter, then $A(\mathbf{k}_\parallel)$ is varied until the convolved function $I(\mathbf{k}_\parallel)$ represents a good fit to the experimental data. Although a full deconvolution is, in principle, possible it is much more straightforward to begin with an assumption for the functional form of $A(\mathbf{k}_\parallel)$ and systematically vary the parameters until a good fit is found. The functional form of $A(\mathbf{k}_\parallel)$ is assumed to be a Lorentzian, the most commonly used photoemission line shape, which results from the $\mathbf{k}$-independent approximation for $\mathrm{Im}[\Sigma(\mathbf{k},\omega)]$.[44]

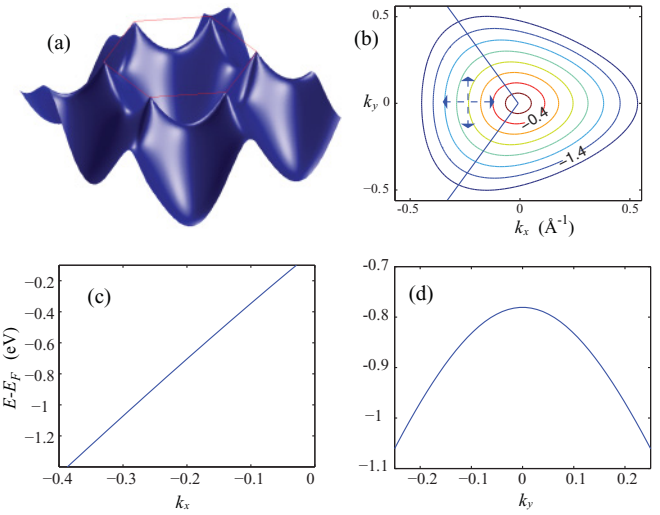

FIG. 6. (Color online) (a) Graphene band structure over first BZ. (b) Contour lines drawn along constant binding energies in the vicinity of the K point (binding energies indicated in eV). (c),(d) Dispersion along k_x and k_y, respectively [along dashed blue lines in (b)].

In carrying out this procedure, we introduce two additional simplifications. First, note that we are examining the region in $\mathbf{k}$ space within the first Brillouin zone along the ΓK (k_x) direction in the vicinity of the K point. As shown in Fig. 6, the π state disperses rapidly along k_x in this region, but relatively slowly along k_y since $\partial\omega/\partial k_y = 0$ at $k_y = 0$. Thus although Eq. (6) describes a 2D convolution, it is possible to replace the required 2D $k_x k_y$ integral with a 1D integral along k_x. Second, we note that most of the MDCs considered here have an asymmetric peak shape, with additional spectral weight in the $\omega > v_F|\mathbf{k}|$ region of the curve. Possible reasons for this asymmetry are discussed in a separate paragraph below. For fitting purposes, this additional spectral weight was not considered and the best fit was obtained by imposing a momentum cutoff within 0.1 Å^{-1} of the peak position on the $\omega > v_F|\mathbf{k}|$ side of the curve. Figure 7(a) shows a representative curve from the $\hbar\omega = 50$-eV data taken 0.7 eV below the Fermi level along with a best fit. Note that the line shape of this curve provides an excellent fit to the experimental data. Figure 7(b) shows the two independent contributions to the linewidth: the corrugation-induced broadening and the intrinsic broadening. In order to cross check that the convolution procedure accurately captures the photon-energy dependence of the photoemission process, the same fitting procedure was repeated on data obtained with a photon energy of $\hbar\omega = 84$. At this photon energy, $k_\perp = 4.27$ Å^{-1} and, according to Eq. (6), the width of $S_{k_\perp}$ is nearly twice as large as it is at $\hbar\omega = 50$ eV.

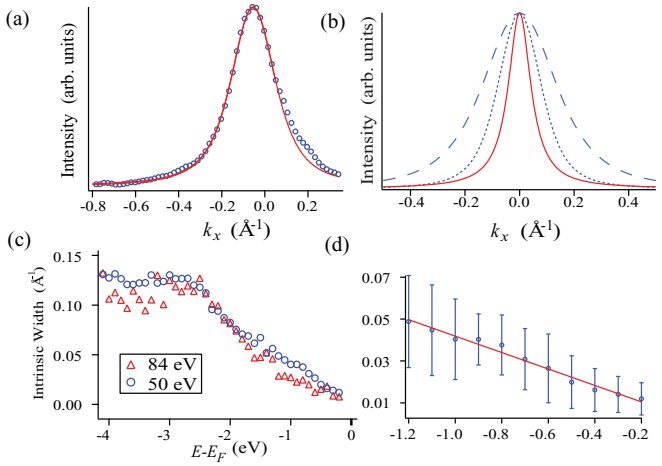

FIG. 7. (Color online) Intrinsic width of ARPES features for suspended monolayer graphene. (a) Example of MDC fitting. Blue circles represent experimental MDC. Solid red line indicates best fit. (b) Two independent contributions to broadening. Solid red line: intrinsic linewidth of initial state. Broken blue lines: broadening due to corrugation at $\hbar\omega = 50$ eV (dotted) and $\hbar\omega = 84$ eV (dashed). (c) Inverse lifetime as a function of binding energy for $\hbar\omega = 50$ (blue circles) and $\hbar\omega = 84$ eV (red triangles). (d) Best-fit line to intrinsic width vs binding energy for $\hbar\omega = 50$ data in vicinity of Fermi level.

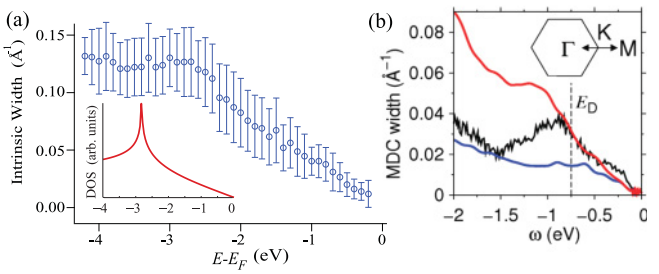

FIG. 8. (Color online) Inverse lifetime as a function of binding energy for $\hbar\omega = 50$ (blue) shown with error bars. Inset shows graphene DOS. (b) Previous experimental and theoretical results for ARPES MDC width of graphene. Plot includes first-principles calculation of Park *et al.* (Ref. 45) for suspended (upper red curve) as well as SiC supported (lower blue curve) graphene along with data from Bostwick *et al.* (Ref. 5) (intermediate black curve). Note that these data correspond to *doped* graphene.

However, as expected, the intrinsic linewidth extracted from the fitting procedure is the same for data obtained with both photon energies. A comparison of the self-energy extracted from the two data sets is shown in Fig. 7(c); the two resulting curves are the same, within experimental error, thus confirming the photon-energy dependence given in Eq. (6) and lending further support to our approach.

Comparison can be made to the theoretical work of Park *et al.* who compute, from first principles, the MDC broadening expected in an ARPES study of graphene.[45] Although their computation has been performed for doped graphene, their result for suspended graphene compares very favorably to ours. Figure 8 shows our result for the intrinsic MDC width along with the prediction of Park *et al.* for both freely suspended graphene and SiC supported graphene. As seen in Fig. 8(b), dielectric screening from the SiC substrate significantly reduces the MDC broadening. However, their result for suspended graphene is qualitatively similar to ours; they predict a monotonic increase in MDC width from 0 at E_F to ∼0.09 at 2 eV. However, care must be taken when comparing this calculation to our result, as the calculation has been performed for doped graphene, which changes the quasiparticle dynamics. For example, the kink observed in the 1–1.5-eV range is not present in our data. In comparison, our measured intrinsic linewidth increases linearly from E_F to ∼3 eV, after which it is constant at ∼0.13 Å^{-1}. The kink at ∼3 eV in our data corresponds to the rapid change in the density of states in graphene, which occurs at a binding energy equal to the nearest-neighbor hopping energy of ∼2.8 eV (see inset to Fig. 8).

To make our observations quantitative, we perform a linear fit of the intrinsic width versus binding energy, $\Gamma_i = \alpha + \beta(E - E_F)$. From this fit, we find $\alpha = 0.002 \pm 0.005$ Å^{-1} and $\beta = 0.039 \pm 0.01$ Å^{-1} eV^{-1}. As expected, the value of α is within experimental uncertainty of zero since excited states just above the Fermi level should be very long lived. Consider now the parameter β that describes the increase in inverse quasiparticle lifetime with increasing binding energy.

The lifetime is related to Γ_i by $\tau = 1/(2\Gamma_i v_F)$. Thus our measured value can be reexpressed as $\beta = 0.78 \pm 0.02$ fs^{-1} eV^{-1}, so as to enable ready comparison with prior measurements of the same quantity on graphite and exfoliated graphene. For graphite, β has been measured by fs photoemission to be an order of magnitude smaller, viz. 0.029 fs^{-1} eV^{-1},[46] while scanning tunneling spectroscopy (STS) measurements of exfoliated graphene on graphite have produced an intermediate value of ($\beta = 0.11$ fs^{-1} eV^{-1}).[47] A reasonable explanation for this discrepancy is the greater out-of-plane corrugation of suspended graphene, which has been predicted to be the largest contribution to electron scattering in rough graphene sheets.[48–50] Indeed, such roughness constitutes short-range correlated disorder, which has also been shown theoretically to lead to scattering rates which scale linearly with ω in graphene.[51]

Comparison can also be made with results obtained on epitaxial graphene grown on SiC. In such a system the Dirac point is 0.5–0.75 eV below the Fermi level which changes the quasiparticle dynamics resulting in a nonlinear behavior for Γ_i vs ω. In particular, it has been shown that electron-plasmon interaction in doped epitaxial graphene results in an increase in the electron-scattering rate in a narrow energy region where $\omega \sim E_D$[5] [see black curve in Fig. 8(b)]. However, at deeper binding energies a nearly linear increase of Γ_i has been demonstrated with a slope of ∼0.025 Å^{-1} eV^{-1}, which is comparable to our measured value of β.

Because of the unique Dirac fermion behavior and two dimensionality of graphene, there has been much discussion of many-body physics that would lead to lifetime broadening in ARPES measurements of graphene.[5,52–54] In conventional bulk crystals Fermi-liquid theory predicts the decay of a photohole through creation of an electron-hole pair to result in a lifetime that scales as $(E - E_F)^2$, in proportion to the number of excitation pathways that satisfy momentum and energy conservation. However, the linear dispersion of the

graphene bands along with the vanishing density of states at E_F modify this picture. Hence undoped graphene is expected to show anomalous marginal Fermi-liquid behavior, characterized by a lifetime that scales as $(E - E_F)^{-1}$.[52] Electron-phonon interaction has also been shown experimentally to lead to linewidth broadening.[5,55] However, the interaction is limited by the phonon dispersion to within 140 meV of E_F.[9] Coulombic interactions, however, can affect scattering rates for electrons well below E_F. As noted above, elastic scattering due to short-range correlated impurities such as adatoms, dislocations, or corrugations has also been shown theoretically to produce a $(E - E_F)^{-1}$ dependence on lifetime.[51]

As discussed above, prior STS measurements have confirmed this linear increase for a small range of energies (∼150 meV) in the vicinity of the Fermi level for exfoliated graphene on graphite.[47] Our measurement confirms that this behavior persists as far as 2 eV below the Fermi level; a log-log plot of Γ_i vs ω displays a slope of ∼1. As noted above, such marginal Fermi-liquid behavior has also been observed by fs time-resolved photoemission spectroscopy on graphite.[46]

We now return to the topic of asymmetry in MDC peak shape. As many recent theoretical studies have pointed out, the commonly made **k**-independent approximation for $\mathrm{Im}[\Sigma(\mathbf{k},\omega)]$ is not fully valid in graphene as the doping level approaches zero.[52,53] The vanishing density of states at $\omega = E_F$ along with graphene's linear dispersion near E_F places a kinematic restriction on the available phase space for electron-electron scattering. The scattering pathway $e^- \rightarrow e^- + e^- h^+$ is only available for off-shell electrons for which $\omega > v_F|\mathbf{k}|$ and is kinematically forbidden when $\omega < v_F|\mathbf{k}|$. Thus one expects a discontinuity in $\mathrm{Im}[\Sigma(\mathbf{k},\omega)]$ at $\omega = k$ and decay due to electron-electron interaction may be indicated by asymmetry in MDC peak shape.[51,53] As mentioned above and indicated in Fig. 7, in MDCs taken through the K point for monolayer graphene additional spectral weight is present in the $\omega > v_F|\mathbf{k}|$ regime. In principle, a full deconvolution of the ARPES intensity would recover the exact function form of $A(\mathbf{k},\omega)$. However, such a procedure would require use of the full 2D integral specified by Eq. (2), which is beyond the scope of the work presented here.

V. SUMMARY

Photoemission on thin sheets of 2D crystals is expected to grow in importance as interest in single layer insulators and semiconductors increases. We have performed ARPES on a 2D suspended surface with well defined surface corrugation. By comparing our work with our prior results obtained from diffraction measurements on corrugation in suspended graphene sheets[14] we have developed a model for understanding the effect of corrugation on ARPES spectra. By analyzing results obtained with different photon excitation energies, we have estimated the contribution of surface roughness to broadening. Thus despite the surface corrugation in the graphene layer, it is still possible to develop insights into graphene physics. In particular, we have shown that exfoliated suspended graphene is essentially undoped in its pristine form. Additionally, we have shown that the band structure has no significant deviations from linearity in the vicinity of the Dirac point. Our measured Fermi velocity is comparable to results obtained on supported graphene by transport and optical measurements. Finally, we have also shown that undoped exfoliated graphene behaves as a marginal Fermi liquid with an anomolous carrier lifetime, which scales as $(E - E_F)^{-1}$.

ACKNOWLEDGMENTS

K.R.K. acknowledges support for materials and sample preparation from NSF Grant No. CHE-0641523 and by NYSTAR; R.M.O. and K.R.K. acknowledge support from DOE BES (Contract No. DE-FG02-04-ER-46157) for experimental work. K.R.K. and R.M.O. acknowledge support from NSF Grant No. 0937683 for travel. The synchrotron portion of the project (A.M., D.C.) at Elettra was supported also through Grant No. PRIN2008-prot.20087NX9Y7_002. A.M. gratefully acknowledges the NSEC at Columbia University and the Italian Academy at Columbia University for the warm hospitality and financial support during his visit. The authors also thank Matthew Foster and Mark Hybertsen for several extensive and helpful discussions.

APPENDIX

In this Appendix, we will follow the standard formalism for single-photon photoemission using the dipole approximation. We will adapt the treatment to deal with a locally curved surface using a specific initial state described by the tight-binding model for graphene.

According to the standard tight-binding scheme, initial π states in the valence band of graphene with energy ω_k and crystal-momentum $\mathbf{k}$ are represented as a linear combination of molecular p_z orbital states:

$$\psi_{\mathbf{k}}(\mathbf{r}) = \frac{1}{\sqrt{N}} \sum_{\mathbf{R}} e^{i\mathbf{k}\cdot\mathbf{R}} \sum_{j=A,B} C_j^{\mathbf{k}} \phi(\mathbf{r} - \mathbf{R} - \tau_j), \qquad \text{(A1)}$$

where $\frac{1}{\sqrt{N}}$ is an overall normalization factor, A and B designate the sublattice sites, and τ_j are their locations within the unit cell. The $C_j^{\mathbf{k}}$ are complex coefficients obtained from the tight-binding model and the ϕ are molecular p_z orbitals. The sum over $\mathbf{R}$ runs over all N unit cells in the crystal (note that we work in the limit where $N \rightarrow \infty$).

The transition matrix for photoexcitation from this initial state to a plane-wave final state with total momentum $\mathbf{k_f}$ outside the crystal can be written, using the dipole approximation, as follows:

$$M^{\mathbf{k}} \propto \int d^3 r e^{-i\mathbf{k}_f\cdot\mathbf{r}} (\mathbf{p}\cdot\mathbf{A}) \psi_{\mathbf{k_i}}(\mathbf{r}) \qquad \text{(A2)}$$

Inserting the above definition for the initial state we obtain

$$M^{\mathbf{k}} \propto (\mathbf{k_i}\cdot\hat{\lambda}) \sum_R e^{i(\mathbf{k_i}-\mathbf{k_f})\cdot\mathbf{R}} \tilde{\phi}(k_f) \sum_{j=A,B} C_j^{\mathbf{k}} e^{-i\mathbf{k_f}\cdot\tau_j}, \qquad \text{(A3)}$$

where $\tilde{\phi}$ is the Fourier transform of the molecular p_z orbital and $\hat{\lambda}$ represents the polarization vector of the incoming radiation. We are interested in a small region of momentum space in the vicinity of the K point. Since $\mathbf{k_i}\cdot\hat{\lambda}$ and $\tilde{\phi}(\mathbf{k_f})$ are nearly constant in this region, we concentrate our attention on the sum, $\sum e^{i(\mathbf{k_i}-\mathbf{k_f})\cdot\mathbf{R}} \sum C_j^{\mathbf{k_i}} e^{-i\mathbf{k_i}\cdot\tau_j}$. The sum over j, $\sum C_j^{\mathbf{k_i}} e^{-i\mathbf{k_f}\cdot\tau_j}$

depends only on the relative phase between the $C_j^{\mathbf{k}}$'s and the path length difference from atoms A and B to the detector. This term changes rapidly on a contour around the K point. Along the ΓK direction, the term changes from 2 to 0 as we pass through the K point from the first to the second BZ. However, if we restrict ourselves to the region of $\mathbf{k}$ space along the ΓK direction within the first BZ (see Fig. 6), $\sum C_j^{\mathbf{k_i}} e^{-i\mathbf{k_f}\cdot\tau_j}$ is nearly constant. Thus we are left with the sum $\sum e^{i(\mathbf{k_i}-\mathbf{k_f})\cdot\mathbf{R}}$.

For a 3D crystal with perfect translational symmetry $\mathbf{R} = n_1\mathbf{a_1} + n_2\mathbf{a_2} + n_3\mathbf{a_3}$ where n_1,n_2,n_3 are integers and $\mathbf{a_1},\mathbf{a_2},\mathbf{a_3}$ are primitive lattice vectors. In this case, the sum over $\mathbf{R}$ reduces to momentum preserving δ function $\delta(\mathbf{k_f} - \mathbf{k_i} - \mathbf{G})$ where G is a reciprocal-lattice vector. However, since graphene is a two-dimensional lattice, momentum conservation does not hold in the perpendicular direction. More significantly, exfoliated graphene is a flexible membrane that is not atomically flat, so the $\mathbf{R}$'s must be expressed in terms of a continuous variable; thus $\mathbf{R} = n_1\mathbf{a}_1 + n_2\mathbf{a}_2 + \Delta x + \Delta y + z$, where z_j is a continuous variable which represents the local height of the graphene sheet. The variation in height is such that we can consider the well-known theory of scattering from continuous rough surfaces in order to evaluate the sum in Eq. (A3). We begin by replacing the discrete sum with an integral:

$$\sum_{\mathbf{R}} e^{i(\mathbf{k_i}-\mathbf{k_f})\cdot\mathbf{R}} = \int d^3r\, D(\mathbf{r}) e^{i(\mathbf{k_i}-\mathbf{k_f})\cdot\mathbf{r}}, \tag{A4}$$

where $D(r)$ is the density function of the material, which, for a perfectly crystalline flat sample, has the form

$$D(\mathbf{r}) = \sum_{\mathbf{R}} \delta(\mathbf{r} - \mathbf{R}). \tag{A5}$$

A periodic lattice generates a photoemission spectrum with the periodicity of the reciprocal lattice. However, since we are concerned with the photoemission spectrum in a small region of $\mathbf{k}$ space in the first Brillouin zone, we may abandon the description of the surface as a discrete lattice and replace it with a smooth, continuous sheet. Thus we approximate $D(r)$ as a surface density function:

$$D(\rho,z') \simeq \delta[z' - z(\rho)], \tag{A6}$$

where $\rho = r_\parallel = (x,y)$ and $z' = r_\perp$. Thus the surface is now defined by the height function $z = z(\rho)$. Inserting the above definition of $D(r)$ and explicitly separating $\mathbf{k_i}$ and $\mathbf{k_f}$ into components parallel and perpendicular to the surface we obtain

$$M \propto \int d^2\rho e^{i(\mathbf{k_{i\perp}}-\mathbf{k_{f\perp}})\cdot z(\rho)} e^{i(\mathbf{k_{i\parallel}}-\mathbf{k_{f\parallel}})\cdot\rho}. \tag{A7}$$

We have retained momentum conservation; for a constant $z(\rho)$ the above integral produces $\delta(\mathbf{k_{i\parallel}} - \mathbf{k_{f\parallel}})$ times a complex phase; but for a nontrivial $z(\rho)$, the δ function broadens since $e^{i(\mathbf{k_{i\perp}}-\mathbf{k_{f\perp}})\cdot z(\rho)}$ is no longer independent of ρ. Additionally, electronic states in graphene propagate on a curved space, which implies that the direction of the initial-state wave vector $\mathbf{k_i}$ varies as a function of position along the surface so that $k_{i\perp}$ and $k_{i\parallel}$ vary with ρ as well. This introduces additional phase variation into the exponential argument $(\mathbf{k_{i\perp}} - \mathbf{k_{f\perp}}) \cdot z(\rho)$. However, this variation is very small in comparison to that introduced by changes in $z(\rho)$ and can effectively be ignored with little change in our final result. In particular, $k_{i\perp}$ varies proportional to $k\frac{\partial z}{\partial \rho_k}$, which is on the order of 0.01 Å^{-1}. Thus the phase variation in the term $k_{i\perp}z \ll 1$ ($\Delta z \approx 2$ Å) is very small in comparison to the variation in the $k_{f\perp}z$ term ($k_{f\perp}$ ranges from 2.5 to 3.5 Å^{-1}). Thus we will approximate the direction of the initial-state wave vector, $\mathbf{k_i}$, as constant for all points on the surface. This means that $\mathbf{k}$ is not ρ dependent and we can define a new vector $\mathbf{k} = \mathbf{k_i} - \mathbf{k_f}$, so that our expression becomes

$$M \propto \int d^2\rho e^{i\mathbf{k}_\perp\cdot z(\rho)} e^{i\mathbf{k}_\parallel\cdot\rho}. \tag{A8}$$

To find the photoemission intensity we use Fermi's golden rule which yields

$$I = \frac{2\pi}{\hbar}\|M\|^2\delta(\epsilon + \hbar\omega - \hbar^2k^2/2m), \tag{A9a}$$

$$\|M\|^2 \propto \int d^2\rho' d^2\rho e^{i\mathbf{k}_\perp\cdot z(\rho)} e^{i\mathbf{k}_\parallel\cdot\rho} e^{-i\mathbf{k}_\perp\cdot z(\rho')} e^{-i\mathbf{k}_\parallel\cdot\rho'}. \tag{A9b}$$

Defining $r = \rho - \rho'$ we can rearrange to obtain

$$I \propto \int d^2r \left(\int d^2\rho e^{i\mathbf{k}_\perp\cdot[z(\rho+r)-z(\rho)]} \right) e^{i\mathbf{k}_\parallel\cdot r}. \tag{A10}$$

The term inside the parentheses is the height difference function, $C(r,k_\perp)$, of the surface, which is related to the height-height correlation function, $H(r) = \langle|z(r_0 + r) - z(r_0)|^2\rangle$. It is straightforward to show that the $C(r,k_\perp)$ equals $e^{-(1/2)H(r)k_\perp^2}$.[43] Thus we have

$$I \propto \int d^2r C(k_\perp,r) e^{i\mathbf{k}_\parallel\cdot r}, \tag{A11a}$$

$$C(k_\perp,r) = e^{-(1/2)H(r)k_\perp^2}. \tag{A11b}$$

For a large class of surfaces, $H(r)$ has the following properties:

$$H(r) \propto e^{2\alpha}, \quad \text{for} \quad r \ll \xi, \tag{A12}$$

$$H(r) = 2w^2, \quad \text{for} \quad r \gg \xi, \tag{A13}$$

where α is a measure of the small scale roughness termed the "roughness exponent." In, particular, it can be shown that the full width at half maximum (FWHM) of $I(k_\parallel)$ (with $k_\perp$ held constant) scales as $\xi^{-1}(wk_\perp)^{1/\alpha}$ when $(wk_\perp)^2 \gg 1$. The functional form of $I(k_\parallel)$ is well approximated as[43]

$$S_{k_\perp}(\mathbf{k}_\parallel) = [\xi/(wk_\perp)^{1/\alpha}]F_\alpha[\mathbf{k}_\parallel\xi/(wk_\perp)^{1/\alpha}]$$

$$F_\alpha(Y) = \int XdX\exp(-X^{2\alpha})J_0(XY). \tag{A14}$$

The above discussion began with the assumption that the initial state ψ_k had a well defined pseudomomentum k and energy ω_k. To include initial-state broadening in our description, we replace ψ_k with a sum over multiple momentum states, $\sum a_k\psi_k$, where the a_k are complex coefficients. The coefficients a_k are related to the spectral function $A(k,\omega)$ by $|a_k|^2 = A(k,\omega)$ with the spectral function defined as

$$A(k,\omega) = \frac{\mathrm{Im}(\Sigma)}{[\omega_k - \omega - \mathrm{Re}(\Sigma)]^2 + \mathrm{Im}(\Sigma)^2}, \tag{A15}$$

where $\Sigma = \Sigma(k,\omega)$ is the quasiparticle self-energy. Retaining our simple description of the final state as a free-electron state with momentum q, our transition matrix

becomes a sum, $M = \sum a_k M^{kq}$, over multiple matrix elements weighted by the complex coefficients a_k, where the M^{kq} are the original transition matrix elements defined in Eq. (A3). Again, using Fermi's golden rule we find that the transition probability is proportional to the square of this sum:

$$I \propto |M|^2 = \left| \sum_k a_k M^{kq} \right|^2 = \sum_k |a_k|^2 |M^{kq}|^2 + \sum_{k \neq k'} a_k^* a_{k'} M^{kq*} M^{k'q}. \quad \text{(A16)}$$

The cross terms have the form

$$M^{kq*} M^{k'q} \propto \int d^2 r \left(\int d^2 \rho e^{i \mathbf{k}_\perp \cdot [z(\rho + r) - z(\rho)]} e^{i \Delta \mathbf{k}_\parallel \rho} \right) e^{i \mathbf{k'}_\parallel \cdot r}, \quad \text{(A17)}$$

where $\Delta \mathbf{k}_\parallel = \mathbf{k'}_\parallel - \mathbf{k}_\parallel$, $\mathbf{k}_\perp \approx \mathbf{k'}_\perp$. The $e^{i \Delta \mathbf{k}_\parallel \rho}$ factor in the ρ integral introduces a random phase that causes the integral to average to zero (since it is taken over the whole surface). Thus the cross terms can be safely neglected and we arrive at the final expression or photoemission intensity as a function of $k_\parallel$ with $k_\perp$ fixed, described by Eq. (2).

[1] K. Novoselov, A. Geim, S. Morozov, D. Jiang, M. Grigorieva, S. Dubonos, and A. Firsov, Nature (London) **438**, 197 (2005).

[2] Y. Zhang, Y. Tan, H. Stormer, and P. Kim, Nature (London) **438**, 201 (2005).

[3] A. Neto, F. Guinea, N. Peres, K. Novoselov, and A. Geim, Rev. Mod. Phys. **81**, 109 (2009).

[4] T. Ohta, A. Bostwick, T. Seyller, K. Horn, and E. Rotenberg, Science **313**, 951 (2006).

[5] A. Bostwick, T. Ohta, T. Seyller, K. Horn, and E. Rotenberg, Nat. Phys. **3**, 36 (2006).

[6] Y. S. Dedkov, M. Fonin, U. Rüdiger, and C. Laubschat, Phys. Rev. Lett. **100**, 107602 (2008).

[7] A. M. Shikin, G. V. Prudnikova, V. K. Adamchuk, F. Moresco, and K. H. Rieder, Phys. Rev. B **62**, 13202 (2000).

[8] A. L. Vázquez de Parga, F. Calleja, B. Borca, M. C. G. Passeggi Jr., J. J. Hinarejos, F. Guinea, and R. Miranda, Phys. Rev. Lett. **100**, 056807 (2008).

[9] Y. Liu, L. Zhang, M. K. Brinkley, G. Bian, T. Miller, and T. C. Chiang, Phys. Rev. Lett. **105**, 136804 (2010).

[10] I. Pletikosić, M. Kralj, P. Pervan, R. Brako, J. Coraux, A. T. NDiaye, C. Busse, and T. Michely, Phys. Rev. Lett. **102**, 056808 (2009).

[11] P. Sutter, M. Hybertsen, J. Sadowski, and E. Sutter, Nano Lett. **9**, 2654 (2009).

[12] T. Valla, J. Camacho, Z. H. Pan, A. V. Fedorov, A. C. Walters, C. A. Howard, and M. Ellerby, Phys. Rev. Lett. **102**, 107007 (2009).

[13] M. Sprinkle *et al.*, Phys. Rev. Lett. **103**, 226803 (2009).

[14] K. R. Knox, S. Wang, A. Morgante, D. Cvetko, A. Locatelli, T. O. Mentes, M. A. Niño, P. Kim, and R. M. Osgood Jr., Phys. Rev. B **78**, 201408 (2008).

[15] K. Bolotin, K. Sikes, Z. Jiang, M. Klima, G. Fudenberg, J. Hone, P. Kim, and H. Stormer, Solid State Commun. **146**, 351 (2008).

[16] F. Wang, Y. Zhang, C. Tian, C. Girit, A. Zettl, M. Crommie, and Y. Shen, Science **320**, 206 (2008).

[17] K. Mak, M. Sfeir, J. Misewich, and T. Heinz, Proc. Natl. Acad. Sci. USA **107**, 14999 (2010).

[18] Y. Fujikawa, T. Sakurai, and R. M. Tromp, Phys. Rev. B **79**, 121401 (2009).

[19] V. Geringer, M. Liebmann, T. Echtermeyer, S. Runte, M. Schmidt, R. Ruckamp, M. C. Lemme, and M. Morgenstern, Phys. Rev. Lett. **102**, 076102 (2009).

[20] M. Ishigami, J. Chen, W. Cullen, M. Fuhrer, and E. Williams, Nano Lett. **7**, 1643 (2007).

[21] A. Locatelli, K. Knox, D. Cvetko, T. Menteş, M. Niño, S. Wang, M. Yilmaz, P. Kim, R. Osgood Jr., and A. Morgante, ACS Nano **4**, 4879 (2010).

[22] E. Stolyarova, K. Rim, S. Ryu, J. Maultzsch, P. Kim, L. Brus, T. Heinz, M. Hybertsen, and G. Flynn, Proc. Natl. Acad. Sci. USA **104**, 9209 (2007).

[23] W. G. Cullen, M. Yamamoto, K. M. Burson, J. H. Chen, C. Jang, L. Li, M. S. Fuhrer, and E. D. Williams, Phys. Rev. Lett. **105**, 215504 (2010).

[24] A. Locatelli, A. Bianco, D. Cocco, S. Cherifi, S. Heun, M. Marsi, M. Pasqualetto, and E. Bauer, J. Phys. IV (France) **104**, 99 (2003).

[25] T. Schmidt, S. Heun, J. Slezak, J. Diaz, K. Prince, G. Lilienkamp, and E. Bauer, Surf. Rev. Lett. **5**, 1287 (1998).

[26] A. Locatelli and E. Bauer, J. Phys.: Condens. Matter **20**, 093002 (2008).

[27] A. Locatelli, L. Aballe, T. Mentes, M. Kiskinova, and E. Bauer, Surf. Interface Anal. **38**, 1554 (2006).

[28] H. Hibino, H. Kageshima, F. Maeda, M. Nagase, Y. Kobayashi, and H. Yamaguchi, Phys. Rev. B **77**, 075413 (2008).

[29] M. Altman, J. Phys.: Condens. Matter **17**, S1305 (2005).

[30] E. L. Shirley, L. J. Terminello, A. Santoni, and F. J. Himpsel, Phys. Rev. B **51**, 13614 (1995).

[31] S. Hüfner, *Photoelectron Spectroscopy: Principles and Applications* (Springer-Verlag, Berlin, 2003).

[32] A. R. Law, M. T. Johnson, and H. P. Hughes, Phys. Rev. B **34**, 4289 (1986).

[33] S. Zhou, G. Gweon, J. Graf, A. Fedorov, C. Spataru, R. Diehl, Y. Kopelevich, D. Lee, S. Louie, and A. Lanzara, Nat. Phys. **2**, 595 (2006).

[34] K. Sugawara, T. Sato, S. Souma, T. Takahashi, and H. Suematsu, Phys. Rev. Lett. **98**, 036801 (2007).

[35] A. Grüneis *et al.*, Phys. Rev. Lett. **100**, 037601 (2008).

[36] S. D. Kevan and R. H. Gaylord, Phys. Rev. B **36**, 5809 (1987).

[37] J. Meyer, A. Geim, M. Katsnelson, K. Novoselov, T. Booth, and S. Roth, Nature (London) **446**, 60 (2007).

[38] F. Theilmann, R. Matzdorf, and A. Goldmann, Surf. Sci. **420**, 33 (1999).

[39] F. Theilmann, R. Matzdorf, G. Meister, and A. Goldmann, Phys. Rev. B **56**, 3632 (1997).

[40] It is implied here that Δx, Δy, and z are functions of position along the surface with z representing the local height of the surface and Δx, Δy representing deviations from the ideal lateral positions of surface atoms, which are necessary to keep the average bond length unchanged.

[41]T. Lu and M. Lagally, Surf. Sci. **120**, 47 (1982).
[42]H. N. Yang, T. M. Lu, and G. C. Wang, Phys. Rev. Lett. **68**, 2612 (1992).
[43]H. Yang, G. Wang, and T. Lu, *Diffraction from Rough Surfaces and Dynamic Growth Fronts* (World Scientific, Singapore, 1993).
[44]In fitting the MDCs an instrumental broadening term was also convolved with our spectral function. The energy resolution introduces a width of $\Delta E v_F$, which is approximately 0.042 $Å^{-1}$. Additionally, as discussed in the text, the momentum resolution of the instrument (known from prior calibration) is 0.045 $Å^{-1}$.
[45]C. Park, F. Giustino, C. Spataru, M. Cohen, and S. Louie, Nano Lett. **9**, 4234 (2009).
[46]S. Xu, J. Cao, C. C. Miller, D. A. Mantell, R. J. D. Miller, and Y. Gao, Phys. Rev. Lett. **76**, 483 (1996).
[47]G. Li, A. Luican, and E. Y. Andrei, Phys. Rev. Lett. **102**, 176804 (2009).
[48]D. Gazit, Phys. Rev. B **79**, 113411 (2009).
[49]E. Mariani and F. von Oppen, Phys. Rev. Lett. **100**, 076801 (2008).
[50]M. Katsnelson and A. Geim, Philos. Trans. A **366**, 195 (2008).
[51]M. S. Foster and I. L. Aleiner, Phys. Rev. B **77**, 195413 (2008).
[52]S. Das Sarma, E. H. Hwang, and W. K. Tse, Phys. Rev. B **75**, 121406 (2007).
[53]J. Gonzalez, F. Guinea, and M. A. H. Vozmediano, Phys. Rev. Lett. **77**, 3589 (1996).
[54]J. Gonzalez, F. Guinea, and M. A. H. Vozmediano, Phys. Rev. B **63**, 134421 (2001).
[55]Z. Li, E. Henriksen, Z. Jiang, Z. Hao, M. Martin, P. Kim, H. Stormer, and D. Basov, Nat. Phys. **4**, 532 (2008).